

Homonuclear NMR Correlations between Half-Integer Quadrupolar Nuclei Undergoing Magic-Angle Spinning

Mattias Edén[†] and Lucio Frydman*

Chemical Physics Department, Weizmann Institute of Science, Rehovot 76100, Israel

Received: June 24, 2003; In Final Form: October 8, 2003

This study presents a theoretical, numerical, and experimental survey on the nature of homonuclear dipolar couplings in systems of half-integer quadrupolar nuclei undergoing magic-angle-spinning (MAS). Various spin interactions that do not commute with homonuclear dipolar couplings (chemical shift effects, heteronuclear dipolar couplings, quadrupolar interactions) may lead to recoupling effects under MAS, yielding a variety of pathways for transferring magnetization between proximate quadrupole nuclei in 2D correlation experiments. The Hamiltonians underlying this anisotropy-driven recoupling of the dipolar interactions are theoretically derived and their characteristics revealed from theoretical and numerical arguments. To explore when and how these various recoupling mechanisms become relevant, a variety of ²³Na and ¹¹B 2D exchange NMR experiments were performed at different external magnetic fields and MAS frequencies on several compounds: Na₂HPO₄·2H₂O, Na₂SO₃, disodium deoxycytidine heptahydrate, B₂O₃ and B₁₀H₁₄. The structural information content afforded by these experiments as well as their potential limitations are discussed.

1. Introduction

Recent years have witnessed a surge in the application of solid-state nuclear magnetic resonance (NMR) techniques on nuclei possessing a spin $S > 1/2$.^{1–4} Such nuclei are usually affected by intense quadrupolar interactions arising from the surrounding electric field gradients (EFGs), which may affect NMR line shapes through first- as well as second-order effects.^{1–7} The renewed interest in this kind of spectroscopy has been driven by the important roles that such species play in a variety of technologically important materials, by advances in NMR instrumentation, as well as by a better understanding about the spatial and spin properties of quadrupole-related effects. As a result of these factors a number of alternatives have been proposed and demonstrated for the routine acquisition of high-resolution solids NMR spectra from half-integer quadrupoles.^{6–12} Yet as the use of solid state quadrupolar NMR expands, limitations in our current ability to extract structural information from multiple-spin systems involving quadrupolar nuclei become evident. The present paper deals with a simple route that could potentially be useful for gaining connectivity, internuclear distance, and molecular geometry information in systems of quadrupolar nuclei, based on spontaneous recoupling processes arising when these spins are subject to magic-angle-spinning (MAS).

The measurement and interpretation of dipolar couplings constitutes a well-established approach to extract structural information from solids.^{13–15} These experiments are usually carried out in combination with MAS of the sample, an approach that for dilute spin-1/2 nuclei can afford high-resolution spectra. As this procedure will remove, among other first-order anisotropies, the dipolar couplings needed for establishing the spin–spin connectivities, a considerable number of dipolar recoupling

techniques capable of selectively bringing back the dipolar couplings have been developed for spin-1/2 systems.^{16–18} Most of these employ sequences of radio frequency (rf) pulses that are synchronized with the sample rotation, pulses that need to be characterized by rates of spin nutation much larger than the internal interactions within the spin system. However, though this strong rf requirement can often be met for dilute spins 1/2, it will not in general hold for $S \geq 1$ systems affected by potentially strong quadrupolar interactions. A number of low rf power alternatives have been recently demonstrated for achieving homonuclear dipolar recoupling between half-integer quadrupolar nuclei,^{19,20} though research in this area is still considerably less developed than that of spin-1/2.

Given the challenges arising when relying on rf pulse sequences to achieve homonuclear recoupling between quadrupolar nuclei, attention has also been focused on alternatives capable of achieving this recoupling without rf. Rotational resonance under MAS as well as off-magic-angle spinning experiments, count among the approaches that have been explored recently.^{21–23} Another potential recoupling approach relies on letting other anisotropic interactions within the spin system drive the homonuclear recoupling.^{24–33} As we have encountered this source for spontaneous recoupling of practical interest for monitoring homonuclear connectivities in quadrupolar spin systems, we decided to describe some of their aspects in this publication. Toward this end we begin by summarizing in the coming section the overall form of the anisotropy-driven recoupling, and the different mechanisms capable of driving such recoupling between half-integer quadrupoles. The recoupling efficiency under various idealized conditions is also investigated with the aid of numerical simulations. A results-based section follows, where compounds and experimental conditions were chosen to illustrate various aspects of these recoupling processes. Finally, we briefly discuss the relative merits and shortcomings of experiments that rely solely on such unassisted recoupling processes.

* Corresponding author. E-mail: Lucio.Frydman@weizmann.ac.il.

[†] Present address: Physical Chemistry Division, Arrhenius Laboratory, Stockholm University, SE-106 91 Stockholm, Sweden.

2. Spontaneous Recoupling: Theory and Simulations

Spin Hamiltonian. The rotating frame spin Hamiltonian for two homonuclear half-integer quadrupolar spins (S_j and S_k) coupled to N_1 spin- $1/2$ (denoted I) and undergoing MAS, may be written as

$$H(t) = H_{\text{CS}}(t) + H_{\text{D}}^{\text{IS}}(t) + H_{\text{D}}^{\text{SS}}(t) + H_Q(t) \quad (1)$$

The first term represents the chemical shift Hamiltonian, which for simplicity we shall assume affects only the observed S spins. This in turn may be expressed as an orientation- and time-independent part $H_{\text{CS}}^{\text{iso}}$, plus an orientation- and time-dependent chemical shift anisotropy (CSA)

$$H_{\text{CS}}^{\text{aniso}}(t) = \omega_j^{\text{aniso}}(t)S_{jz} + \omega_k^{\text{aniso}}(t)S_{kz} \quad (2)$$

where $\omega_j^{\text{aniso}}(t)$ is the anisotropic chemical shift frequency of spin j . The second term in eq 1 represents the Hamiltonian of the heteronuclear couplings between each of the quadrupolar nuclei and the surrounding I spins, which we assume is only mediated through space:

$$H_{\text{D}}^{\text{IS}}(t) = \sum_{i=1}^{N_1} \omega_{ij}^{\text{IS}}(t) 2I_{iz}S_{jz} + \omega_{ik}^{\text{IS}}(t) 2I_{iz}S_{kz} \quad (3)$$

Likewise, the homonuclear Hamiltonian between spins j and k

$$H_{\text{D}}^{\text{SS}}(t) = \omega_{jk}^{\text{SS}}(t) \frac{1}{\sqrt{6}} \left(2S_{jz}S_{kz} - \frac{1}{2} S_j^+ S_k^- - \frac{1}{2} S_j^- S_k^+ \right) = \omega_{jk}^{\text{SS}}(t) T_{20}^{jk} \quad (4)$$

involves solely a dipolar coupling frequency ω_{jk}^{SS} times the T_{20}^{jk} second-rank irreducible spherical tensor operator. Finally, the last term in eq 1 is specific to $S > 1/2$ nuclei, as it represents the interaction between the nuclear spins and electric field gradients in their surroundings. Here we shall express this Hamiltonian in a perturbative expansion, whose first-order term is given by

$$H_Q^{(1)}(t) = \omega_j^Q(t) \frac{1}{\sqrt{6}} (3S_{jz}^2 - S(S+1)) + \omega_k^Q(t) \frac{1}{\sqrt{6}} (3S_{kz}^2 - S(S+1)) = \omega_j^Q(t) T_{20}^j + \omega_k^Q(t) T_{20}^k \quad (5)$$

$\omega_j^Q(t)$ is the quadrupolar frequency, directly proportional to the frequency $\chi_Q/2\pi = C_Q/2S(2S-1)$, where $C_Q = e^2 Q \hbar$ is the quadrupolar coupling constant. The second-order quadrupolar Hamiltonian is given by

$$H_Q^{(2)}(t) = \sum_{m=1,2} \omega_j^{(2)m}(t) [T_{2m}^j, T_{2-m}^j] + \sum_{m=1,2} \omega_k^{(2)m}(t) [T_{2m}^k, T_{2-m}^k] \quad (6)$$

The spin commutators in this expression may be decomposed into a sum of first and third-rank irreducible tensors, whereas the second-order quadrupolar frequencies $\omega^{(2)m}$ are proportional to C_Q^2/ω_0 and have components that transform as a sum of zero-, second-, and fourth-rank tensors.^{6,34}

Note that anisotropic terms in eq 1 are time dependent due to the periodic oscillations introduced by MAS. This time dependence may in all cases be expressed as the Fourier series

$$\omega_{\Lambda}(t) = \sum_n \omega_{\Lambda}^{(n)} \exp\{in\omega_r t\} \quad (7)$$

where the various Fourier components $\omega_{\Lambda}^{(n)}$ for $\Lambda = \text{chemical shift, dipolar or quadrupolar}$ interactions are explicitly given in ref 35.

Origin of Anisotropy-Driven Recoupling. As mentioned earlier, the main focus of this paper is the spontaneous recoupling phenomena associated to cross-correlations between the pairwise $S-S$ homonuclear dipolar interaction, and other anisotropic terms in the spin Hamiltonian. This recoupling happens intrinsically within the spin system due to a combination of (i) the noncommutation between the spin part of the homonuclear dipolar coupling T_{20}^{jk} and the spin part T_{Λ} of another anisotropic spin interactions in the Hamiltonian of eq 1, (ii) the fact that the spatial tensor components of these two interactions do not coincide, and (iii) a MAS process which renders all these anisotropic spatial components synchronously time dependent.³⁶ To better visualize the effective Hamiltonian arising from these three conditions, it is convenient to consider the simplified Hamiltonian

$$H(t) = H_{\Lambda}(t) + H_{\text{D}}^{\text{SS}}(t) \quad (8)$$

where $H_{\Lambda}(t)$ is any interaction $\{H_{\text{CS}}^{\text{aniso}}(t), H_{\text{D}}^{\text{IS}}(t), H_Q^{(1)}(t), H_Q^{(2)}(t)\}$ that can potentially fulfill condition (i). The effective recoupling can be derived by entering an interaction frame generated by the interaction Λ . This transforms the Hamiltonian in eq 8 according to

$$\tilde{H}(t) = \exp\{i \int_0^t dt' \omega_{\Lambda}^{\text{aniso}}(t') T_{\Lambda}\} H(t) \times \exp\{-i \int_0^t dt' \omega_{\Lambda}^{\text{aniso}}(t') T_{\Lambda}\} \quad (9)$$

where $\omega_{\Lambda}^{\text{aniso}}(t')$ is the time-dependent frequency of interaction Λ (eq 7). This transformation effectively removes $H_{\Lambda}(t)$ from $H(t)$ but imposes a time dependence on the spin part of H_{D}^{SS} , $T_{20}^{jk} \rightarrow \tilde{T}_{20}^{jk}(t)$, which may be expressed as a closed set of q operators $\{T_{20}^{jk} \times T_{\Lambda}\}_q$. Their precise expressions depend on the commutation properties between T_{20}^{jk} and T_{Λ} but are not important for our qualitative description: explicit expressions for the interference between some of them may be found in the literature.^{26,30,37,38} Here we formally rewrite them as

$$\tilde{T}_{20}^{jk}(t) = \sum_{n=-\infty}^{\infty} \sum_q f_q^{(n)} \exp\{in\omega_r t\} \{T_{20}^{jk} \times T_{\Lambda}\}_q \quad (10)$$

The weighting coefficients $f_q^{(n)}$ in eq 10 are in turn proportional to the Fourier coefficients $\{a_{\Lambda}^{(n)}\}$ that define the anisotropic Λ interaction under MAS according to

$$\exp\{i \int_0^t dt' \omega_{\Lambda}^{\text{aniso}}(t')\} = \sum_{n=-\infty}^{\infty} a_{\Lambda}^{(n)} \exp\{in\omega_r t\} \quad (11)$$

Combining eqs 4 and 10 we may summarize the effective Hamiltonian in the Λ -driven frame as $\tilde{H}(t) = \omega_{jk}^{\text{SS}}(t) \tilde{T}_{20}^{jk}(t)$, involving the product of two time-dependent terms: one deriving from the spatial term $\omega_{jk}^{\text{SS}}(t)$, which is time dependent due to the action of the MAS, and another deriving from the spin part $\tilde{T}_{20}^{jk}(t)$, which is time dependent due to the transformation imposed by the Λ interaction. Including also the explicit Fourier expansion in eq 7, this effective coupling becomes

$$\tilde{H}(t) = \sum_q \sum_{n=-\infty}^{\infty} \sum_{m=-2}^2 \omega_{jk}^{(m)} f_q^{(n)} \exp\{i(n+m)\omega_r t\} \{T_{20}^{jk} \times T_{\Lambda}\}_q \quad (12)$$

TABLE 1: General Features of Anisotropy-Driven Recoupling Mechanisms

Hamiltonian driving the recoupling	spinning-speed dependence	B_0 dependence
$H_{\text{CS}}^{\text{aniso}}$	yes	yes
H_{D}^{IS}	yes	no
$H_{\text{Q}}^{(1)}$	yes	no
$H_{\text{Q}}^{(2)}$	yes	yes
$H_{\text{QxD}}^{\text{L}}$	no	yes

Equation 12 conveys the “gist” of anisotropy-driven recoupling, as it shows that even if homonuclear dipolar interactions may be averaged out by MAS when taken in isolation, their interference with other anisotropic interactions will lead to time-independent contributions. This follows from employing average Hamiltonian theory (AHT):³⁹ after integrating eq 12 over a rotational period only those terms in with $n = -m$ survive and result in a time-independent recoupled dipolar interaction

$$\langle \tilde{H}(t) \rangle_{\text{cycle}} = \bar{H}_{\text{D}}^{\text{SS}} = \sum_q \sum_{m=-2}^2 \omega_{jk}^{(m)} f_q^{(-m)} \{T_{20}^{jk} \times T_{\Lambda}\}_q \quad (13)$$

Notice that because for exact MAS $\omega_{jk}^{(0)} = 0$, it is the Fourier components $\omega_{jk}^{(m)}$ with $m = \pm 1, \pm 2$ —weighted by the coefficients $f_q^{(-m)}$ —that will define the strength of the recoupling. As the weighting coefficients $\{f_q^{(-m)}\}_{m=\pm 1, \pm 2}$ are in turn functions of the coefficients $a_{\Lambda}^{(m)}$, which correspond to the spectral sideband amplitudes generated by the anisotropic part of the interaction Λ when considered in isolation, it follows that the efficiency of the recoupling varies nonmonotonically as the spinning frequency is increased. Indeed, the size of the $a_{\Lambda}^{(m)}$ coefficients depends on the relative ratio between the anisotropy coupling $\omega_{\Lambda}^{\text{aniso}}$ and the MAS frequency ω_r .^{36,40} The sideband amplitudes $a_{\Lambda}^{(\pm 1)}$ and $a_{\Lambda}^{(\pm 2)}$, and hence also the magnitude of the dipolar recoupling, will be maximized when the spinning frequency is about the same as the anisotropy frequency, i.e., when $|\omega_{\Lambda}^{\text{aniso}}/\omega_r| \approx 1$. In the case of first-order quadrupolar-driven recoupling, studies show that the recoupling is maximized when $|\chi_Q/\omega_r|$ is between 1 and 2.³⁰ At either lower or higher spinning frequency conditions, the efficiency of the recoupling is thus expected to drop.

Qualitative Features of Various Recoupling Mechanisms. Although the anisotropy-driven recoupling is fairly straightforward to describe, realistic analyses become cumbersome because several recoupling mechanisms are usually active simultaneously. Still, certain generalities may be derived, particularly with regard to the spinning speed and magnetic field dependencies that can be expected for various recoupling mechanisms. These are summarized in Table 1 and are briefly addressed in the present paragraph.

Arguably, the most common interaction mediating homonuclear recoupling is the heteronuclear IS dipolar field. This anisotropy is dominant when dealing with couplings between spin- $1/2$ nuclei embedded in protonated solids, and similar effects can be expected when investigating spin-pairs of half-integer quadrupolar nuclei in organic or biological solids. In fact IS-driven recoupling has been exploited in the context of 2D exchange spectroscopy between half-integer quadrupolar spins,^{24,28,31,32} its main characteristics are an independence of the external magnetic field strength, and the possibility of its removal by decoupling of the I nuclei. Further examples are presented below in the Results and Discussion.

Another anisotropy capable of driving the homonuclear recoupling is the CSA. Cases of CSA-driven recoupling have been reported for spin- $1/2$ pairs,^{36,38,41} but to our knowledge have so far not been considered for quadrupolar cases. Several characteristics of this recoupling mechanism are common with those of the heteronuclear IS driven recoupling, even if by contrast to the latter, CSA-driven recoupling will be B_0 -dependent. CSA effects might be important for recoupling quadrupolar spins that are subject to large interactions, such as ^{59}Co . In our experience we have not encountered cases where the extent of this recoupling is significant.

Another source of anisotropy-driven recoupling arises when dealing with multiple S–S homonuclear couplings. In the case of systems experiencing several strong and noncoinciding couplings of this kind, mutual recoupling processes will become active, which MAS will not succeed in averaging out. This situation is familiar in the context of ^1H MAS NMR⁴² and may also occur in homonuclear multispin systems of strongly magnetic quadrupolar nuclei. Experimental examples of such residual dipolar effects are illustrated below.

A source anisotropy that will generally need to be accounted for when considering the recoupling between $S > 1/2$ is that arising from quadrupolar interactions. Because of their wide potential magnitude, it is convenient to subdivide these effects into those arising from first- and from second-order components. Details about how first-order quadrupolar-driven recoupling acts have already been considered on the basis of the formalism given in the preceding paragraph:^{25–27,29,30} they are independent of the external field and most pronounced when the differences between the quadrupolar frequencies of the spin pair are of the same order of magnitude as the sample spinning frequency. In most instances, however, line broadening effects are not visible because quadrupolar frequencies are much larger than ω_r . Still, as exemplified below, quadrupolar-driven recoupling may become a central mechanism in magnetization transfer correlation experiments. As for $H_Q^{(2)}$, the most important difference vis-à-vis the remaining first-order Hamiltonians hitherto discussed arises from its different behavior under MAS. $\omega^{(2)m}$ coupling frequencies in $H_Q^{(2)}$ entail a second-rank part that recouples H_{D}^{SS} in a manner that is analogous to that of the first-order cases but also contain a zero-rank part that is equivalent to an isotropic chemical shift, and a fourth-rank part that will not be refocused by MAS and that exhibits both time-dependent and time-independent components. Without going into a detailed discussion of its effects, we mention that qualitatively, the $H_Q^{(2)}$ -driven recoupling is expected to be similar to that of small first-order interactions.

Another potential source of recoupling is that arising from the laboratory-frame cross-term between the full quadrupolar and dipolar spin Hamiltonians. This second-order Hamiltonian $H_{\text{QxD}}^{\text{L}}$ is formally analogous to the second-order quadrupolar interaction, and thus proportional to $C_Q \omega_{jk}^{\text{SS}}/\omega_0$. As discussed in ref 43, this quadrupolar-dipolar cross-term is small (typically less than 50 Hz) and not usually visible even between directly bonded spins. But it possesses components that are not averaged by MAS, and hence in contrast to all other dipolar recoupling mechanisms discussed so far provides a source of recoupling that is independent of ω_r .

Using only the anisotropic parts of the interactions to analyze dipolar recoupling ignores the important effects that isotropic shifts, arising from chemical shielding as well as from the time-independent parts of the second-order quadrupolar interactions, may introduce. Given the longitudinal character of their spin operators, these time-independent components will not be

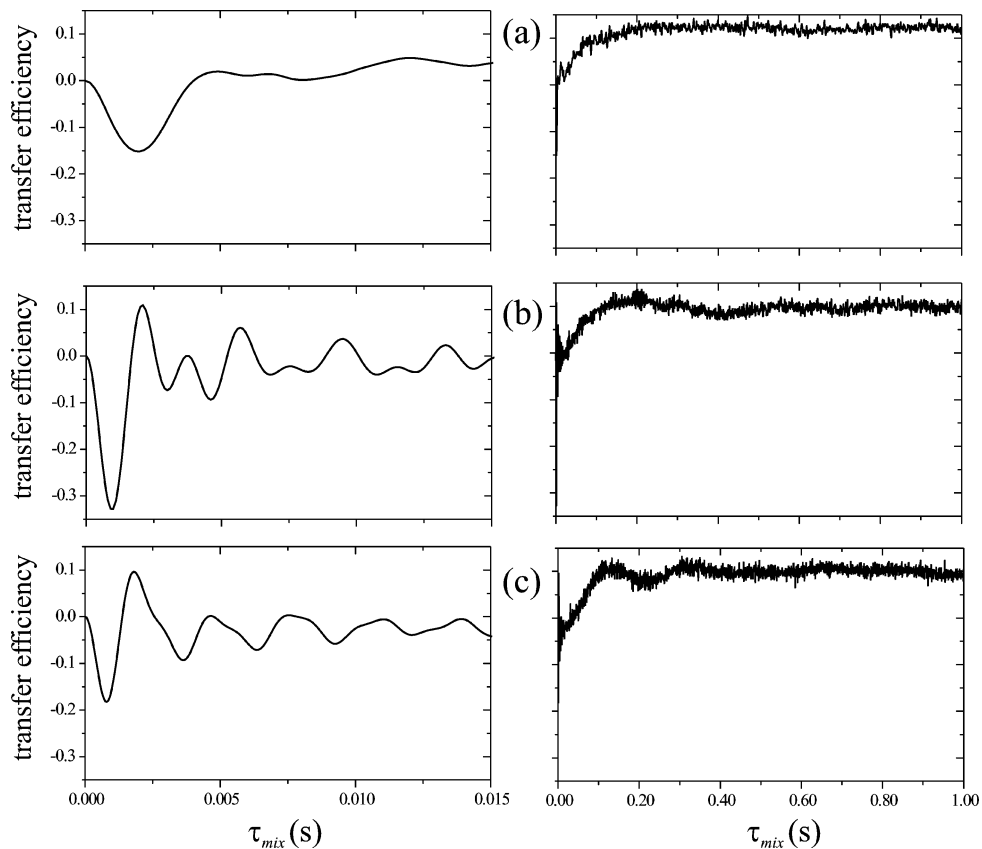


Figure 1. Numerical simulations of magnetization transfers as function of the mixing interval (τ_{mix}) for three spinning frequencies: (a) $\omega_r/2\pi = 5.5$ kHz, (b) 10.0 kHz, and (c) 20.0 kHz. The simulations involved two $S = 3/2$ with coinciding quadrupolar tensors with equal isotropic chemical shifts and quadrupolar coupling constants (100 kHz), placed perpendicularly to the dipolar vector ($b_{jk}/2\pi = -500$ Hz). The Larmor frequency was -132.5 MHz (representative for ^{23}Na quadrupolar sites at a magnetic field of 11.7 T). The left-hand and right-hand panels show the short-term and long-term behavior of the transfers, respectively.

affected by the interaction frame transformation in eq 9. However, because they do not commute with the spin terms of the homonuclear recoupled interaction, they will often lead to truncation effects, which diminish (or sometimes even completely suppress) these dipolar effects. Similar truncation cases of the homonuclear dipolar coupling by isotropic shifts are of course also common among spins $1/2$. The only instance to apparently remove their effects without the aid of rf-driven manipulations arises when arranging for so-called rotational resonance conditions, whereby the spinning speed is adjusted to be equal to an integer multiple of the isotropic chemical shift difference.^{37,44} Rotational resonance has also been explored in the case of half-integer quadrupolar spins;²¹ the main difference with its spin- $1/2$ counterpart stemming in this case from the presence of the anisotropic fourth-rank term in $H_Q^{(2)}$, which provides a time-independent frequency spread even under the action of MAS, as well as time dependencies that oscillate more rapidly than their first-order counterparts.

Numerical Simulations of the Recoupling. Given the numerous sources that can activate the recoupling between half-integer quadrupoles, we decided to probe some of them numerically by simulating magnetization transfers within a pair of $S = 3/2$ spins. The Hamiltonian invoked included the homonuclear S–S dipolar interaction as well as the quadrupole-specific couplings discussed in the preceding paragraphs (other shielding and dipolar anisotropies were not included, as their effects have already been dealt with extensively in spin- $1/2$ investigations^{38,45}). Magnetization transfer curves were then simulated as follows. The time propagator was estimated numerically by a small-step integration of the Schrödinger

equation over one rotational period. An effective Hamiltonian was derived from this period propagator, and a frequency-domain “spectrum” was calculated from its eigenvectors and eigenvalues. The magnetization transfer curve was then obtained by an inverse Fourier transform of this spectrum and is presented as a “transfer efficiency”: the fraction of the initial magnetization being transferred as a function of the mixing time (τ_{mix}). Physically, these curves would correspond to the total cross-peak intensity in a 2D correlation experiment, whereby a transfer efficiency of 1.0 means a complete transfer of the initial magnetization from the central transition of spin j to the central transition of spin k . We verified from COMPUTE calculations⁴⁶ that the stroboscopic sampling at integer multiples of the rotational period that this treatment implies, was also representative for cases of faster sampling.

A large number of simulations involving changing the homonuclear dipolar as well as the two quadrupolar coupling constants and their relative orientations, were performed. The transfer curves obtained were sensitive to all of these parameters; the results presented here are a few cases that we believe are representative for the main trends. These simulations assume a Larmor frequency of $\omega_0/2\pi = -132.5$ MHz, and two symmetric quadrupolar tensors with equal quadrupolar coupling constants and coinciding orientations, but assumed perpendicular to the dipolar vector. Due to the very strong dependence of the recoupling on the isotropic chemical shifts of the two quadrupolar sites, we first discuss the magnetization transfers assuming equal isotropic chemical shifts of the two sites, and next their dependence as the isotropic chemical shift difference is increased.

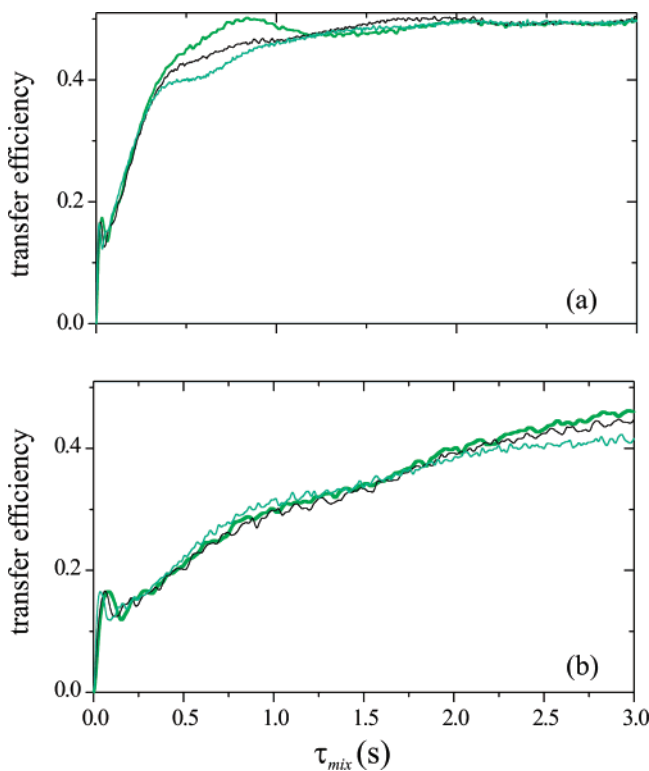


Figure 2. Same parameters as in Figure 1, except that the quadrupolar coupling constants is 2.0 MHz, and $b_{jk}/2\pi$ is equal to (a) -500 Hz and (b) -200 Hz, respectively. Note the similar long-term transfer behavior for all spinning frequencies.

We consider first a case where the spins have equal isotropic chemical shifts. The left panel of Figure 1 shows magnetization

transfer curves calculated as a function of spinning rate, assuming a small quadrupolar coupling ($C_Q/2\pi = 100$ kHz) leading to negligible second-order quadrupolar effects. It is seen that the most efficient transfer (about 30%) is obtained at the intermediate spinning frequency of 10 kHz, which corresponds to the ratio $|\chi_Q/\omega_r| = 1.67$. A nonmonotonic ω_r behavior is characteristic of first-order quadrupolar-driven recoupling, as explained in more detail in ref 30. In that paper, we demonstrated that first-order quadrupolar-driven recoupling may produce line broadening effects in the NMR spectra of quadrupolar spin-pairs. The most pronounced broadening effects (cf., Figure 1 of ref 30) occurred at the same ratio as that maximizing the magnetization transfers discussed here.

Figure 1 also shows that the amplitude of the transferred magnetization may be either positive or negative. The long-term behavior of this transfer is depicted in the right-hand panel of Figure 1 and shows that over a few hundred milliseconds the fraction of the transferred magnetization stabilizes at ca. 10%. This value is essentially independent of the spinning frequency; further simulations indicate that this can be accounted for by an interference between the $H_Q^{(1)}$ and $H_{Q\times D}^L$ terms.

Figure 2a shows the corresponding simulations when all parameters are kept identical, except from using the quadrupolar couplings 2.0 MHz. Given the choice of Larmor frequency, it is expected that $H_Q^{(2)}(t)$ will now play a major recoupling role as well. It is seen that magnetization transfer occurs slowly and that eventually the two spins end up with equal magnetizations. This time there is no fast transfer as in the small C_Q case, but the total transfer is more complete. Further simulations (not shown) also indicate that (i) the asymptotic value depends strongly on the relative orientations between the dipolar and quadrupolar tensors, as well as on the relative orientations

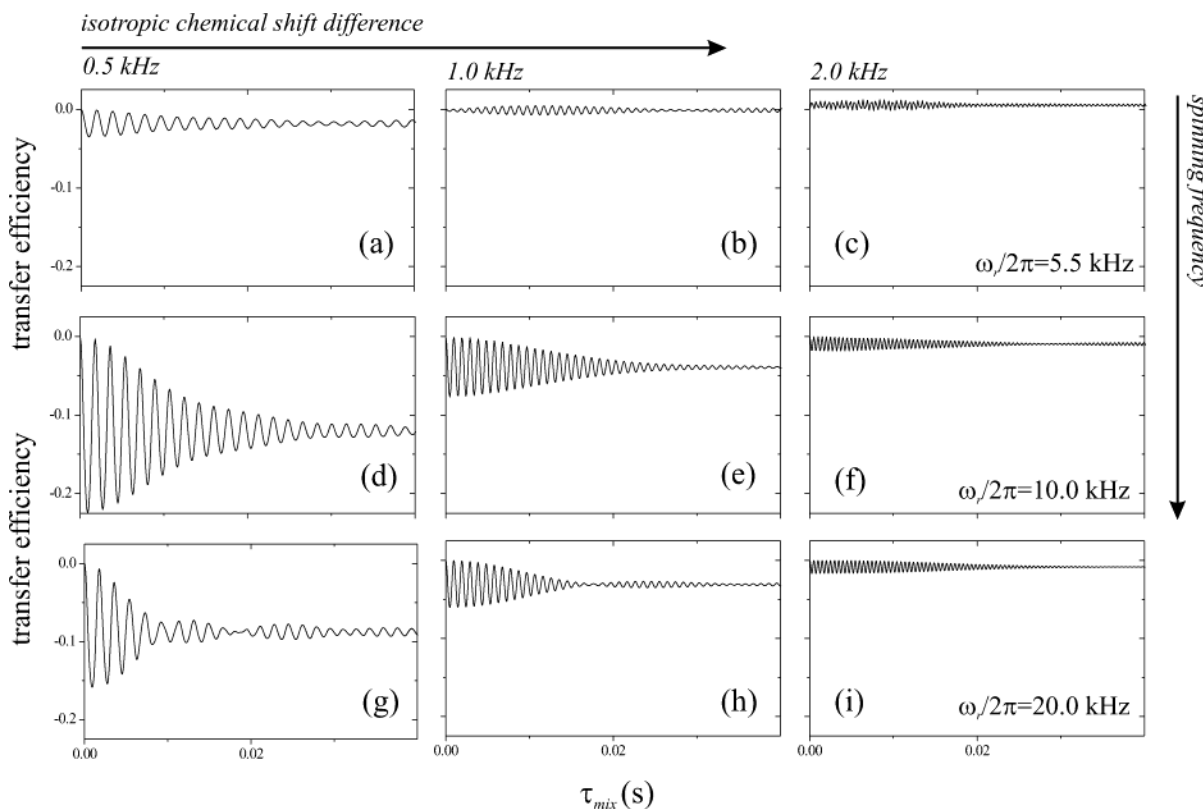


Figure 3. Effects of isotropic chemical shifts on the homonuclear recoupling. The simulation parameters are as in Figure 1, except that differences in isotropic chemical shift are introduced. The array of plots is such that the isotropic chemical shift difference is constant along each column, corresponding to 0.5 kHz (a), (d), (g), 1.0 kHz (b), (e), (h), and 2.0 kHz (c), (f), (i). The spinning frequency is the same along each row and corresponds to $\omega_r/2\pi$ being equal to 5.5 kHz (a)-(c), 10.0 kHz (d)-(f), and 20.0 kHz (g)-(i), respectively.

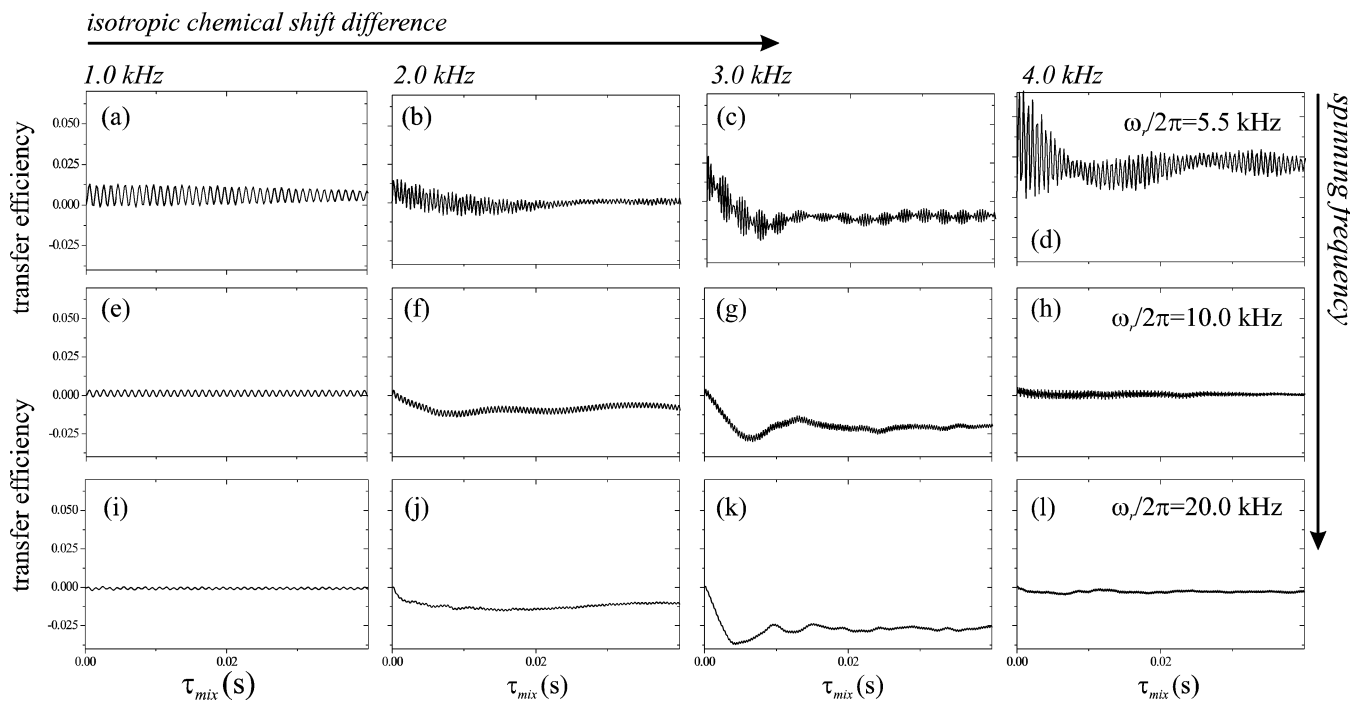


Figure 4. Simulations of magnetization transfer curves as in Figure 2, but including isotropic chemical shifts. The array of plots is such that the isotropic chemical shift difference is constant along each column, corresponding to 1.0 kHz (a), (e), (i), 2.0 kHz (b), (f), (j), 3.0 kHz (c), (g), (k), and 4.0 kHz (d), (h), (l). The spinning frequency is kept constant along each row and corresponds to $\omega_r/2\pi = 5.5$ kHz (a)–(d), 10.0 kHz (e)–(h), and 20.0 kHz (i)–(l), respectively.

between the quadrupolar tensors, and (ii) the speed of transfer depends on the dipolar coupling constant.

Figure 3 shows the same set of simulations as in Figure 1, but now including chemical-shift differences between the two sites. As is seen, even small shift differences decrease markedly the recoupling, whereas large shift differences (not shown) may quench the recoupling further except at rotational resonance conditions. The relative efficiency of the first-order recoupling as a function of the spinning speed, however, is still maintained: the most “efficient” recoupling occurs at $\omega_r/2\pi = 10.0$ kHz, where the rate of sample spinning is comparable to the difference between the sites’ first-order quadrupole coupling. Figure 4 extends the large- C_Q simulations in Figure 2 by including chemical shift differences. The truncation effects of the chemical shift are once again very significant, and these curves also capture the long-term behavior. The most efficient transfer of the cases shown is for $\omega_r/2\pi = 5.5$ kHz and 4.0 kHz difference in isotropic chemical shifts, which is a result of being close to a rotational resonance condition.

A substantial increase in the complexity of the behavior of the transfer curves was noticed upon including the remaining potential anisotropies (CSA, IS dipole couplings) into the simulations of these central transition transfer processes. We also observed that omitting any of the terms arising from the first- and second-order quadrupolar Hamiltonians, as well as from the rather small quadrupolar–dipolar laboratory-frame cross-term, could lead to strikingly different recoupling behaviors. This stresses the need to keep all quadrupole-related terms when exploring homonuclear dipolar effects in quadrupolar spin systems, and the care that needs to be excised upon extrapolating spin- $1/2$ conclusions to quadrupoles even when monitoring solely the latter’s central transitions.

3. Experimental Section

To explore the main features arising from the preceding section experimentally, a series of powdered samples incorpo-

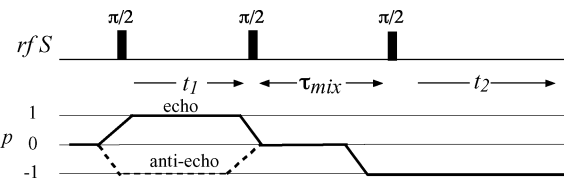


Figure 5. 2D pulse sequence used throughout this paper for monitoring homonuclear dipolar couplings between half-integer quadrupolar spins under MAS conditions. Although not explicitly indicated, high-power ^1H decoupling during various portions of the sequence was carried out as indicated in the text.

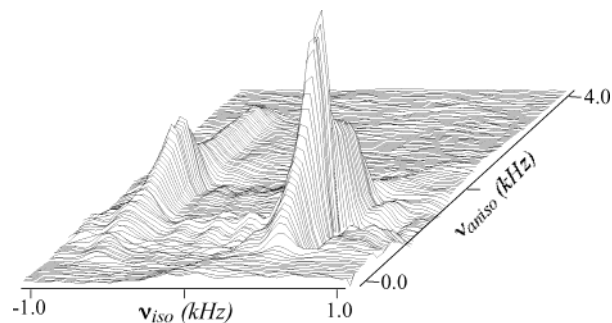


Figure 6. ^{23}Na MQMAS NMR spectrum of $\text{Na}_2\text{HPO}_4 \cdot 2\text{H}_2\text{O}$ recorded at 11.7 T ($\omega_0/2\pi = -132.518$ MHz) and $\omega_r/2\pi = 10.0$ kHz in the presence of TPPM decoupling ($\omega_{\text{nut}}/2\pi = 70$ kHz) during acquisition. The spectrum displays two inequivalent sites. We estimated the quadrupolar and isotropic shift parameters as follows: Site 1: $C_Q = 1.63$ MHz, $\eta = 0.81$, isotropic chemical shift 3.7 ppm (referenced to solid NaCl). Site 2: $C_Q = 2.36$ MHz, $\eta = 0.895$ isotropic chemical shift 4.3 ppm.

rating $S = 3/2$ quadrupolar nuclei were investigated. As in most relevant applications the resulting S–S coupling will remain fairly small, below the limit of line-shape-based detection, an approach relying on 2D exchange NMR spectroscopy^{47–49} was employed in these studies. Figure 5 shows the basic pulse scheme of this experiment, as applied to establishing homo-

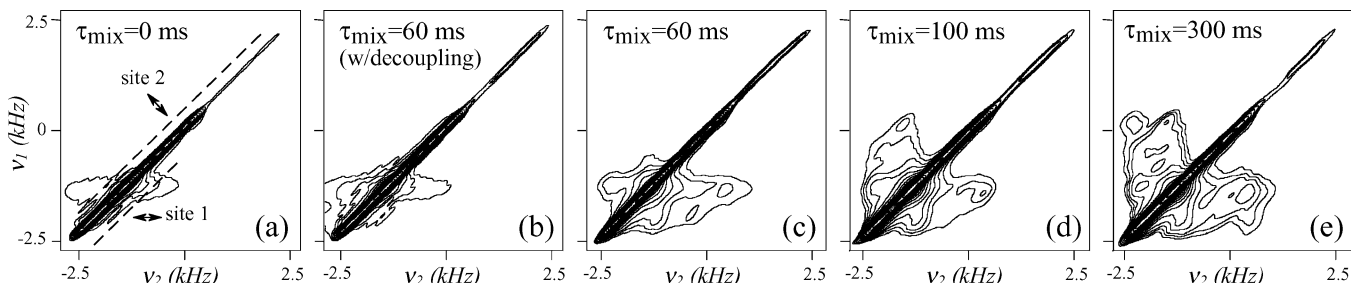


Figure 7. Experimental ^{23}Na 2D exchange spectra recorded for $\text{Na}_2\text{HPO}_4 \cdot 2\text{H}_2\text{O}$ at 7.1 T ($\omega_0/2\pi = -79.88$ MHz) and $\omega_r/2\pi = 5.0$ kHz, for different mixing intervals τ_{mix} . Spectra were acquired in the presence of TPPM decoupling during the t_1 and t_2 evolution intervals and without decoupling during the mixing period, except for the spectrum in (b). Dashed lines in the left-most panel indicate the approximate positions of the powder peaks, as defined by the two line shapes resolved in the corresponding 2D MQMAS NMR spectrum.

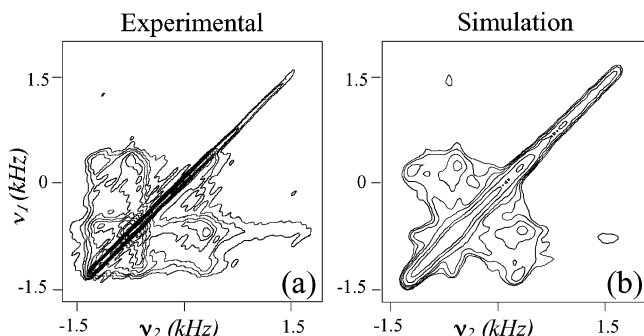


Figure 8. (a) Experimental ^{23}Na 2D exchange spectrum of $\text{Na}_2\text{HPO}_4 \cdot 2\text{H}_2\text{O}$ ($\omega_0/2\pi = -132.518$ MHz). The spectrum was acquired in the presence of TPPM decoupling during the t_1 and t_2 evolution intervals, but without decoupling during mixing. $\omega_r/2\pi = 5.0$ kHz and $\tau_{\text{mix}} = 500$ ms. (b) Powder NMR spectra calculated as indicated in the text, by summation of single-crystal 2D exchange spectrum over 3722 crystal orientations selected according to the ZCW scheme.^{62,63} This numerical simulation employed the quadrupolar and shift parameters given in the caption of Figure 6, with the relative quadrupolar tensor orientation (α, β, γ) = (40°, 35°, 40°). The resulting 2D “stick spectrum” was apodized with a 75 Hz Lorentzian line-broadening in both spectral dimensions.

nuclear correlations between the central transitions of quadrupolar spin systems. If recoupling occurred between spins j and k during the mixing interval a cross-peak will occur at frequency coordinates $(\omega_1, \omega_2) = (\omega^j, \omega^k)$, where ω^j and ω^k are their respective resonance frequencies. As discussed elsewhere, a potential wealth of structural information is available from the resulting 2D line shapes: their presence indicates a nonnegligible dipolar interaction between the nuclear spins, and their rate of buildup informs about the magnitude of the dipolar coupling.^{45,48,49} Furthermore, because the MAS spectra of quadrupolar nuclei are broadened by second-order quadrupolar interactions, the cross-peaks in 2D correlation experiments are in general “featured”; their exact appearance will depend on various quadrupolar parameters including the relative orientations of the quadrupolar tensors of the exchanging sites.^{24,31–33}

Because of the different field dependencies expected from the various anisotropy-driven recoupling mechanisms, NMR spectra were recorded on a variety of laboratory-built spectrometers operating at magnetic fields of 4.7, 7.2, and 11.7 T. Experiments were also repeated as a function of MAS rotation rates, using a home-built probehead based on a 5 mm Doty spinner at 4.7 T, and a commercial Varian/CMX 4 mm probehead at 7.2 and 11.7 T. The targets of these NMR experiments were ^{23}Na (100% natural abundance, $\gamma = 7.08 \times 10^7$ rad $\text{T}^{-1} \text{s}^{-1}$, $\omega_0/2\pi = -132.5$ MHz at 11.7 T), and ^{1}B (80% natural abundance, $\gamma = 8.58 \times 10^7$ rad $\text{T}^{-1} \text{s}^{-1}$, $\omega_0/2\pi = -160.7$ MHz at 11.7 T). Except for the disodium deoxycytidine heptahydrate ($\text{Na}_2\text{dCMP}(5') \cdot 7\text{H}_2\text{O}$, dCMP for short), which was

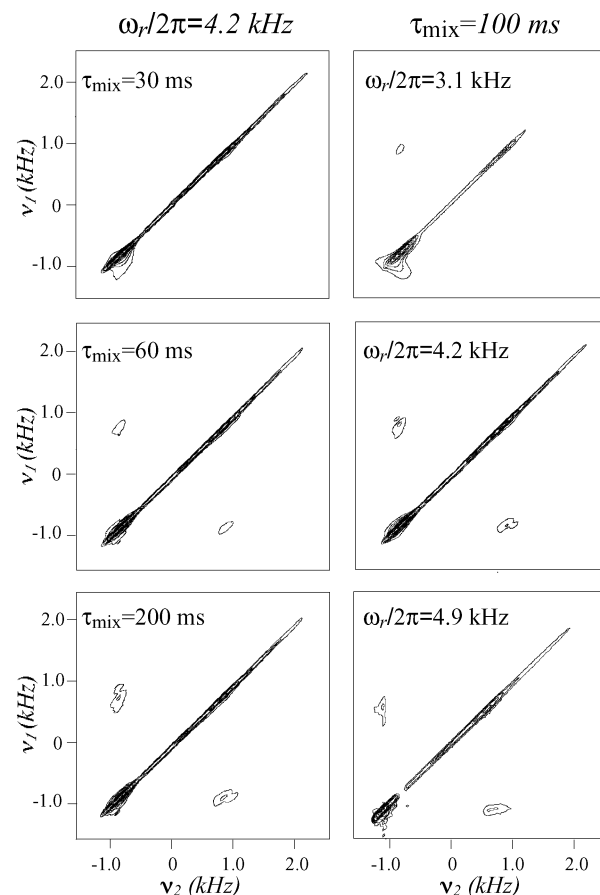


Figure 9. Experimental ^{23}Na 2D exchange spectra acquired on disodium deoxycytidine heptahydrate (dCMP) at 11.7 T using TPPM decoupling during the evolution intervals, but not during mixing. Left-hand column: spectra recorded at the fixed spinning frequency $\omega_r/2\pi = 4.2$ kHz for increasing mixing intervals. Right-hand column: same experimental conditions, except that $\tau_{\text{mix}} = 100$ ms was kept constant and the spinning frequency varied. Note that the rf carrier frequency was offset by 300 Hz when recording the spectrum at $\omega_r/2\pi = 4.9$ kHz, compared to the others.

recrystallized from a mixture of acetone/water, all remaining samples were used as received from the chemical suppliers. In all cases phase-sensitive central-transition 2D line shape spectra with sign discrimination along both spectral dimensions were obtained from hypercomplex processing of two separately acquired experiments with coherence transfer pathways $(0 \rightarrow +1 \rightarrow 0 \rightarrow -1)$ and $(0 \rightarrow -1 \rightarrow 0 \rightarrow -1)$; occasionally, heteronuclear TPPM ^1H decoupling⁵⁰ was also employed.

4. Results and Discussion

Na₂HPO₄·2H₂O. This section describes some examples of 2D homonuclear experiments on quadrupolar spin systems,

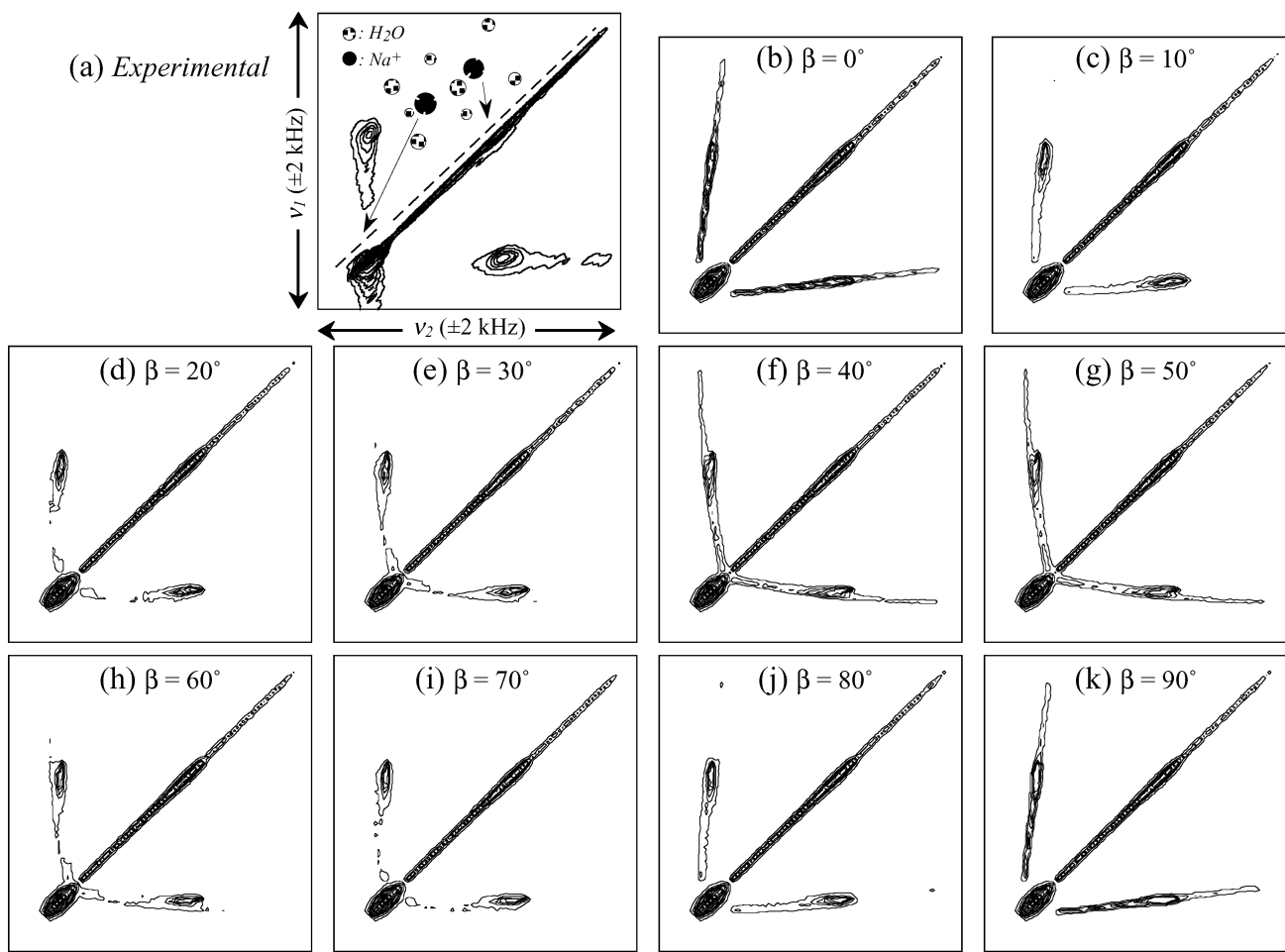


Figure 10. (a) Experimental ^{23}Na 2D exchange spectrum recorded on dCMP at 11.7 T, $\omega_r/2\pi = 4.9$ kHz, and $\tau_{\text{mix}} = 400$ ms. The dashed lines indicate the approximate positions of the powder peaks originated by the chemically distinct sites in the unit cell. (b)–(k) Numerically simulated 2D spectra calculated for different relative quadrupolar tensor orientations and the following spin coupling parameters: Site 1: $C_Q = 0.85$ MHz, $\eta = 0.7$, isotropic chemical shift 0.1 ppm (referenced to solid NaCl). Site 2: $C_Q = 2.3$ MHz, $\eta = 0.9$ isotropic chemical shift -3.9 ppm.⁵³

chosen to illustrate differences between the various prominent dipolar recoupling mechanisms. We begin with an example of a proton-driven magnetization transfer process, as furnished by sodium phosphate dihydrate ($\text{Na}_2\text{HPO}_4 \cdot 2\text{H}_2\text{O}$). This compound crystallizes with two chemically inequivalent sodium sites,⁵¹ which though unresolved in the proton-decoupled ^{23}Na MAS NMR spectrum recorded at $\omega_r/2\pi = 10.0$ kHz and $B_0 = 11.7$ T, can be identified by carrying out an MQMAS acquisition under analogous conditions (Figure 6). From the latter, the quadrupole and chemical shift parameters characterizing the two inequivalent sites can be extracted. Figure 7 shows a series of 2D exchange spectra acquired on this compound at $B_0 = 7.1$ T and $\omega_r/2\pi = 5.0$ kHz, under different conditions. With the mixing time set to zero, the spectrum only displays a main diagonal incorporating the two overlapping ^{23}Na NMR signals (a). A similar result is obtained when a 60 ms mixing interval is utilized in the presence of proton decoupling (b). If the decoupling is turned off during the mixing period, however, off-diagonal exchange signals are visible (c). This indicates correlations between the two ^{23}Na sites, and it may be concluded that homonuclear ^{23}Na – ^{23}Na interactions are recoupled mainly by the presence of heteronuclear ^1H – ^{23}Na interactions. As mixing intervals get longer in the absence of decoupling (d, e), the intensities of the cross-peaks grow into a “mushroom”-shaped pattern. Similar exchange patterns are obtained at a magnetic field of 11.7 T (Figure 8a), as could be expected from the field-independent nature of the dipolar-driven recoupling.

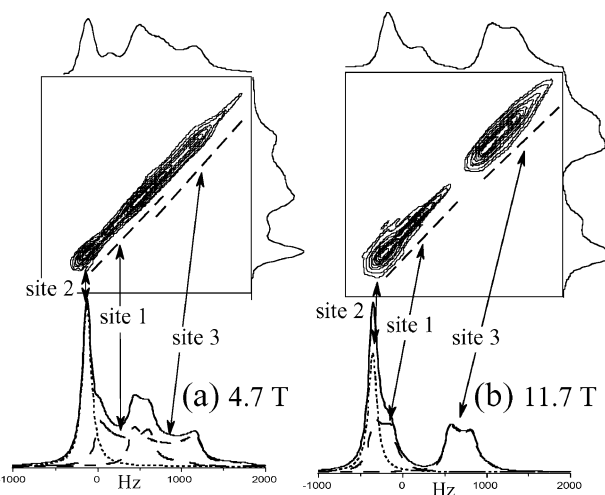


Figure 11. Rationalization of the experimental $\tau_{\text{mix}} = 0$ 2D exchange ^{23}Na MAS NMR spectra of Na_2SO_3 ($\omega_r/2\pi = 4.1$ kHz) recorded at $B_0 = 4.7$ T (a) and 11.7 T (b), on the basis of numerical simulations. Dashed lines in the 2D spectrum denote the resonance regions of sites 1 and 3. In the 1D trace, the solid line represents the total ^{23}Na spectrum and peaks from the individual sites are noted by dashed lines. These were calculated using the following spin coupling parameters. Site 1: isotropic chemical shift -0.8 ppm, $C_Q = 1.10$ MHz. Site 2: isotropic chemical shift -1.4 ppm, $C_Q = 0.24$ MHz. Site 3: isotropic chemical shift -7.5 ppm, $C_Q = 1.14$ MHz. All quadrupole asymmetry parameters $\eta = 0$. The isotropic chemical shifts and quadrupolar parameters were taken from ref 56, and modified slightly to give a best-fit.

Judging from the steady-state reached by the exchange patterns of these spectra, one can conclude that the longest-mixing 2D patterns in Figure 7 have reached the “full-exchange” regime. As explained elsewhere, such spectra may be devoid of detailed information regarding the strength of the homonuclear coupling or the mechanism driving the recoupling, yet carry valuable details about the relative orientations subtended by the quadrupolar tensors of the two exchanging sites.^{45,48,49} One way to extract this information is by simulating sets of 2D exchange spectra as a function of the tensors’ geometry. Such calculations were carried out in the present study as follows: for each crystallite orientation the central-transition 1D MAS resonance positions were calculated for each inequivalent quadrupolar site using the COMPUTE algorithm,⁴⁶ and employing all ancillary relevant information (spinning frequency, isotropic chemical shifts, and first- and second-order quadrupolar interactions; J-couplings and anisotropic chemical shifts were ignored) available for the j, k pair of spins. Arrays of amplitude-frequency pairs (a_m^j, ω_m^j) , with ω_m^j and a_m^j being the m th frequency value and the corresponding spectral amplitude at the coordinate, were thus calculated for each site j . Frequency values were then used to form various two-dimensional histograms of frequency pairs $(\omega_1, \omega_2) = \{(\omega_m^j, \omega_n^j), (\omega_n^k, \omega_m^j), (\omega_m^j, \omega_n^k)$ and $(\omega_n^k, \omega_n^j)\}$, whereas the 2D spectral amplitudes a_{mn}^{jk} associated with each pair of frequencies (ω_m^j, ω_n^k) was calculated according to $a_{mn}^{jk} = w^{jk} a_m^j a_n^k$. The weight w^{jk} accounts for the relative amount of magnetization transferred between sites j and k , and was adjusted empirically using a fixed value for all crystallites so as to provide a reasonable match with the experimental spectrum. The amplitudes for the nonexchanging portions of the magnetizations, a_{mn}^{jj} and a_{nn}^{kk} , were also calculated accordingly. This approach amounts to taking full account of the time dependence of the NMR interactions during the evolution intervals, but treating the magnetization transfer process during the mixing interval phenomenologically. Figure 8b shows such a best-fit simulation for the experimental 11.7 T $\text{Na}_2\text{HPO}_4 \cdot 2\text{H}_2\text{O}$ pattern, as estimated with Euler angles between neighboring quadrupole tensors $(\alpha, \beta, \gamma) = (40^\circ, 35^\circ, 40^\circ)$, and each of these angles having an uncertainty of $\pm 20^\circ$.

dCMP. The disodium salt of deoxycytidine-5'-monophosphate heptahydrate (dCMP) provides another, less trivial test case for exploring quadrupolar spin-diffusion. dCMP presents two distinct ^{23}Na powder patterns, distinguishable even by conventional MAS and arising from proximate sites that differ in their water coordination environments.⁵² The quadrupolar and isotropic chemical shift parameters for these two sites have been recently reported.^{52,54} Figure 9 shows 2D exchange spectra recorded on this compound at 11.7 T in the absence of ^1H decoupling during the mixing, for various spinning frequencies and mixing intervals. At $\omega_r/2\pi = 4.2$ kHz and $\tau_{\text{mix}} = 30$ ms there is no appreciable magnetization exchange, and all signals are concentrated along the diagonal. As the mixing interval is increased, intersite exchange peaks starts building up (Figure 9, left-hand panel). In the presence of ^1H decoupling these peaks vanish (data not shown), and one can thus once again attribute the recoupling as being proton-driven. Notice, however, that the intensity of the exchanged signal is here much weaker than in the case of the sodium phosphate. A different aspect of this ^1H -driven exchange process is illustrated on the right panel of Figure 9. These spectra were recorded at a fixed mixing interval of 100 ms and for different spinning frequencies: $\omega_r/2\pi = 3.1, 4.2$, and 4.9 kHz. Their cross-peak intensities grow as the spinning speed increases, indicating an overall increased efficiency in the ^1H -driven recoupling. This behavior, though

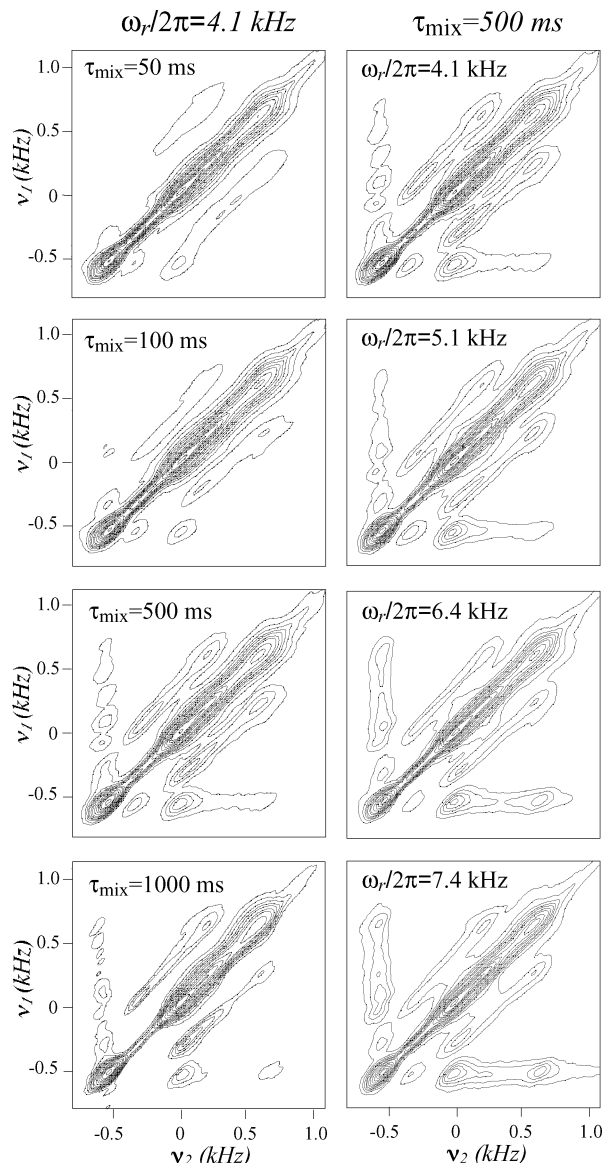


Figure 12. Experimental ^{23}Na 2D exchange spectra on Na_2SO_3 recorded at $B_0 = 4.7$ T and various spinning frequencies and mixing intervals. Left panel: the spinning frequency was kept constant at $\omega_r/2\pi = 7.4$ kHz and the mixing interval was varied. Right panel: the spinning frequency was varied, keeping a constant $\tau_{\text{mix}} = 500$ ms.

unusual, agrees with the general predictions given in the preceding section for a moderately strong IS heteronuclear coupling driving the recoupling. Figure 10a focuses on dCMP’s 2D ^{23}Na NMR exchange spectrum recorded at $\omega_r/2\pi = 4.9$ kHz and $\tau_{\text{mix}} = 400$ ms. Given the longer mixing in this experiment the exchange peaks are slightly more featured, opening up the possibility of establishing relative quadrupolar tensor orientations. Panels b–k in this figure are numerical simulations employing the literature coupling parameters and varying only the angle β_{12} between the two principal axes of the two quadrupolar tensors. Although the data quality is not high enough to enable an unambiguous determination of the relative tensors’ orientations, the best agreement between the features in the experimental and simulated spectra appeared within the ranges $20^\circ \leq \beta_{12} \leq 30^\circ$ and $60^\circ \leq \beta_{12} \leq 70^\circ$. However, as too many combinations of the three $(\alpha_{12}, \beta_{12}, \gamma_{12})$ Euler angles gave reasonable fits, we did not pursue a complete systematic search over the whole space of orientations.

Na₂SO₃. A different situation arises in the case of anhydrous Na_2SO_3 . This compound crystallizes with three inequivalent

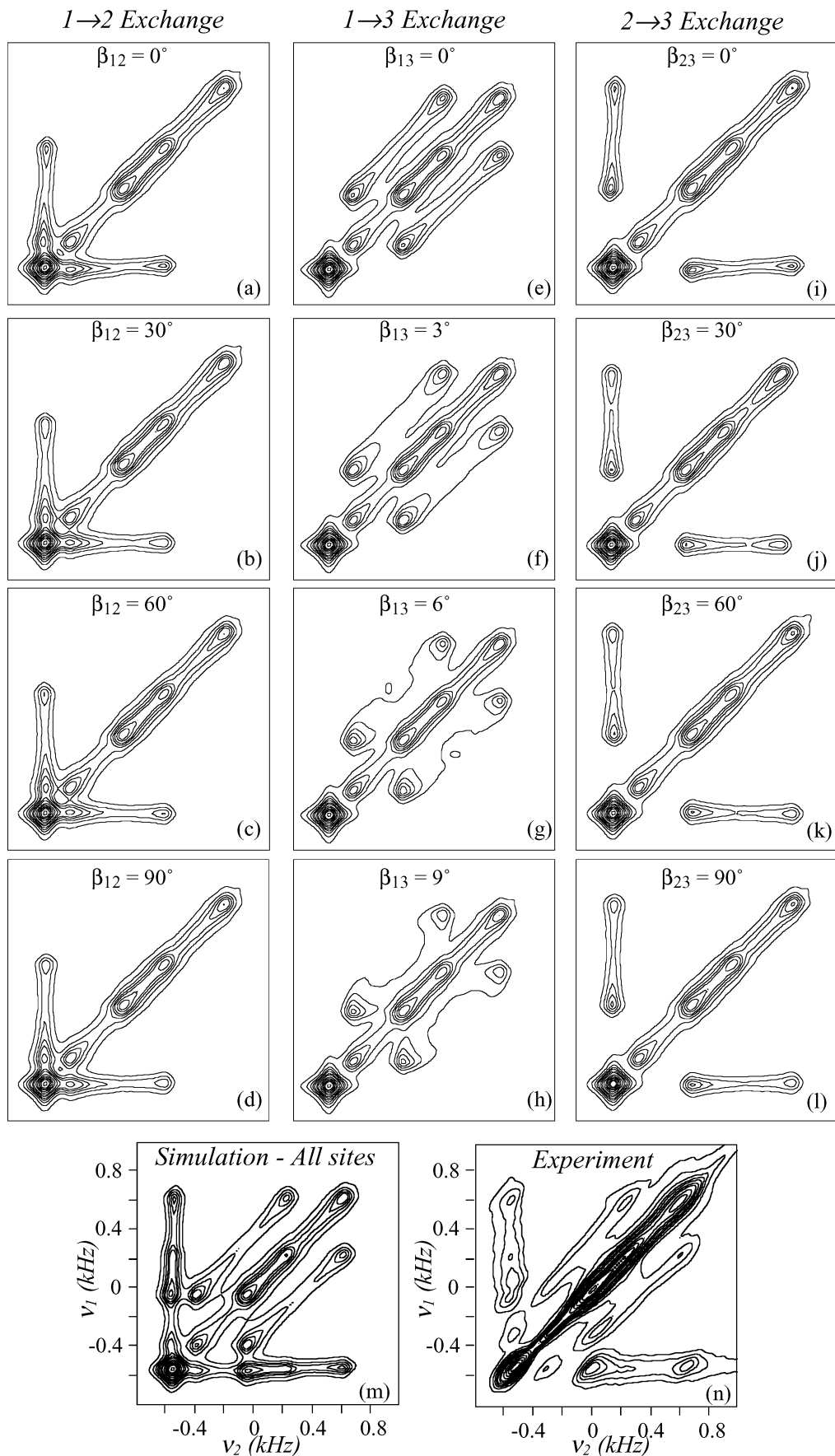


Figure 13. (a)–(m) Numerical simulations of 2D exchange spectra on Na_2SO_3 using the parameters given in Figure 11, $B_0 = 4.7$ T and $\omega_r/2\pi = 7.4$ kHz. The spectra in each of the rows corresponds to (a)–(d) exchange between sites 1 and 2 for different relative quadrupolar tensor orientations β_{12} ; (e)–(h) exchange between sites 1 and 3 for different β_{13} (notice the smaller angular increments); (i)–(l) same as (a)–(d) for the exchange between sites 2 and 3. (m), (n) Comparison between the full simulated and experimental 2D spectra.

sodium sites,⁵⁵ two of them having moderately large ²³Na quadrupolar couplings (≈ 1 MHz), and a third with a much smaller one (≈ 0.24 MHz). The quadrupolar and isotropic shift ²³Na NMR interactions have been determined for this compound using satellite transition MAS and MQMAS,^{10,56} and these can be used to reproduce well the severely overlapped line shapes observed in the conventional MAS spectra observed at $B_0 = 4.7$ T (Figure 11). As there are no protons present in this compound and the spinning frequencies employed in these experiments are ca. 20 times larger than the strongest ²³Na–²³Na coupling in the lattice (286 Hz), the effects of the homonuclear couplings should essentially be completely removed by MAS. Yet as can be appreciated from the left-hand side of Figure 12, residual dipolar couplings lead to an intense magnetization transfer in 2D ²³Na NMR exchange spectra of this compound. In view of its structure, the most likely recoupling mechanism active in this compound should be a MAS modulation of the quadrupolar interaction. To investigate the dependence of this recoupling on the spinning frequency, a series of 2D exchange spectra were acquired at a constant mixing interval $\tau_{\text{mix}} = 500$ ms, for different MAS rates between 4.1 and 7.4 kHz. From these results (Figure 12, right-hand column) one can appreciate that the exchange between sites 1 and 2 stays almost unaffected, the 1–3 exchange is slightly attenuated with increasing MAS rates, whereas the exchange between sites 2–3 is markedly increased. These observations reflect the complicated interplay between the opposing influences that first- and second-order quadrupolar interactions have toward reintroducing homonuclear dipolar couplings between the various sites on changing the rotational frequency of the sample.

The significant cross-peaks revealed by the experimental Na₂SO₃ 2D spectra recorded at $\tau_{\text{mix}} = 500$ ms, can again be targeted to investigate the sensitivity of the spin-diffusion process to the relative tensors orientations. 2D exchange spectra were simulated for each of the three spin-pairs in the crystal (1–2, 1–3, and 2–3), using the axially symmetric ²³Na quadrupolar tensor parameters reported in the literature and varying in consequence only one (β) of the relevant inter-tensor Euler angles. As can be seen from the simulations presented in Figure 13a–d, the exchange patterns between sites 1 and 2 appear to depend very weakly on the orientations of the two tensors. Similar arguments apply for the exchange ridges originating from the 2–3 exchange (Figure 13i–l). The situation is markedly different for the exchanging 1–3 pair (Figure 13e–h), as exchange ridges are parallel to the main diagonal for $\beta_{13} = 0$ but undergo strong deviations even for small variations of β_{13} (note the different ranges of β used in e–h compared to a–d and i–l). From extensive sets of simulations we estimated the relative orientations between tensors 1 and 3 to be $\beta_{13} = 0 \pm 6^\circ$, a highly accurate determination that agrees well with estimates made using a point-charge model.⁵⁶ The superposition of all three exchanging spin patterns and their comparison with the experimentally relevant case are summarized in Figure 13m,n.

B₂O₃. Another interesting target for 2D exchange MAS experiments within half-integer quadrupolar NMR is polycrystalline boron trioxide, B₂O₃. The basic structural units of B₂O₃ in crystalline and glassy phases are planar BO₃ triangles; these appear linked together to form a three-dimensional network which for the most part, about 70%, is made up by interlinked planar boroxol rings composed of three BO₃ units each.⁵⁷ Figure 14 shows 2D ¹¹B exchange spectra collected for different mixing times and at 10 and 14.5 kHz MAS rates at 11.7 T. As may be appreciated, significant cross-peaks develop in these spectra over a time scale of a few hundred milliseconds. Exchange cross-

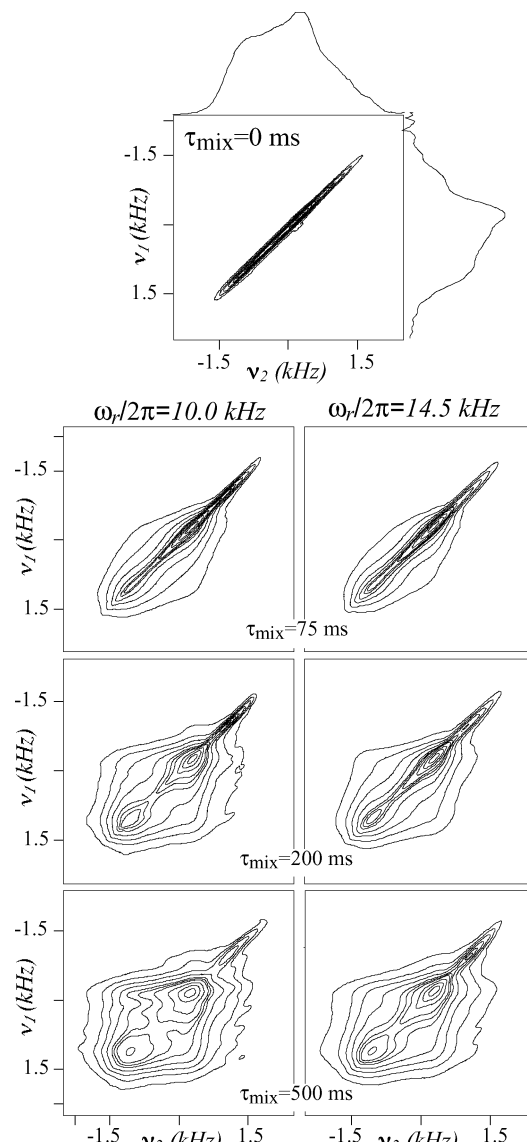


Figure 14. Experimental ¹¹B 2D exchange spectra recorded on boron trioxide (B₂O₃) at $B_0 = 11.7$ T, using the mixing intervals and spinning frequencies indicated.

peaks have also been reported for this compound in variable-angle-spinning experiments,²² where the nonaveraged homonuclear couplings lead to exchange patterns at much shorter (1–2 orders of magnitude) mixing time scales. As in the Na₂SO₃ case, the absence of ¹H's in the structure suggests that this homonuclear recoupling process is quadrupole-driven. Yet the stronger ¹¹B–¹¹B dipolar interactions found in the B–O–B segments of boron oxide systems, also open up the possibility of spin diffusion being driven by multiple noncommuting homonuclear couplings. To distinguish between these two possibilities, magnetization transfer experiments were repeated as a function of magnetic field strength. Most remarkable in these tests was our failure to obtain, at 4.7 T and $\omega_r/2\pi \approx 7$ kHz, any significant off-diagonal intensities (data not shown). Although this is not the kind of variation that one could expect if homonuclear dipolar couplings were to be driving the cross-correlations, such attenuation of the spin-diffusion is consistent with a scenario where moderately intense quadrupolar interactions drive the recoupling. Then, on going to a lower magnetic field, this recoupling process is likely to be quenched due to

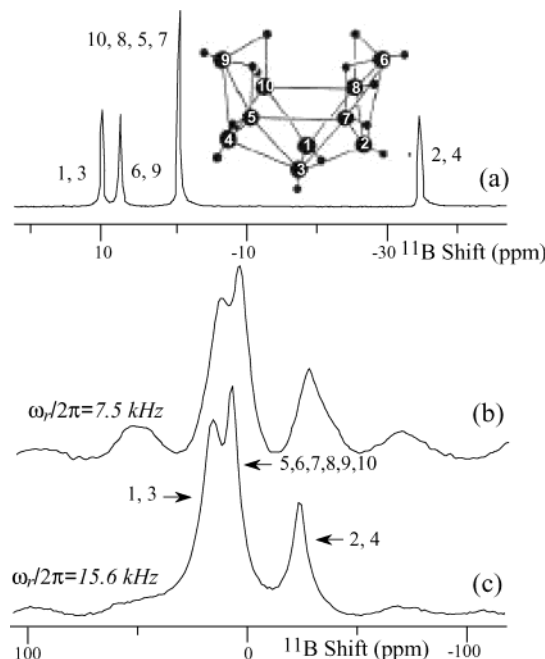


Figure 15. Experimental ^{11}B MAS spectra of decaborane ($\text{B}_{10}\text{H}_{14}$) at $B_0 = 11.7$ T recorded in an *n*-hexane solution (a) and in the solid phase (b), (c), indicating for each case the assignment of the four inequivalent boron sites in the molecule to various peaks. In all experiments ^1H decoupling was used.

the enhanced truncation associated to the increased second-order isotropic quadrupole shift effects.

B₁₀H₁₄. We consider *nido*-decaborane, $\text{B}_{10}\text{H}_{14}$, as a final case in this experimental survey. This boron hydride molecule has a distorted icosahedral shape with ten B atoms occupying its vertexes, ten H atoms directly bonded to each B, and the remaining H atoms forming nonclassical B—H—B three-centered bonds.⁵⁸ Figure 15 illustrates its (labeled) molecular structure, together with ^1H -decoupled solution and MAS solid-state ^{11}B NMR spectra acquired on $\text{B}_{10}\text{H}_{14}$ at 11.7 T. Whereas the four inequivalent ^{11}B sites in the molecule can be clearly resolved in the literature-assigned solution spectrum,⁵⁹ the ^{11}B MAS trace presents three partially overlapping peaks. On the basis of MQMAS and separated-local-field NMR results on this compound, we assign this spectrum as follows:⁶⁰ the most shielded peak (-33 ppm from neat $\text{B}(\text{OCH}_3)_3$) to B^2/B^4 , the center peak at (-3 ppm) originates from a superposition of two inequivalent sites ($\text{B}^5/\text{B}^7/\text{B}^8/\text{B}^{10}$ and B^6/B^9), whereas the signal at 9 ppm corresponds to B^1/B^3 . Figure 16 illustrates a series of experimental 2D exchange MAS NMR spectra collected on this compound as a function of mixing time. As can be appreciated, a significant cross-peak structure develops in this compound within considerable short mixing periods. The presence of an extensive ^1H network in the compound might suggest that this reflects a proton-driven recoupling. However, all spectra in Figure 16a–e were collected using TPPM decoupling throughout the experiment. Further, only minor differences arise upon removing the decoupling from the mixing period. Additionally, the increased extent of spin-diffusion observed upon reducing the sample's MAS rate (Figure 17) also points against a quadrupole-driven source for the recoupling. These features combined suggest that cross-peaks here are driven by the modulation of the multiple homonuclear dipolar couplings experienced by every ^{11}B site, as each pair of bonded borons is subject to a homonuclear coupling of ca. 2.2 kHz (ca. an order of magnitude higher than the strongest couplings observed in the sodium cases). As mentioned in the preceding section this

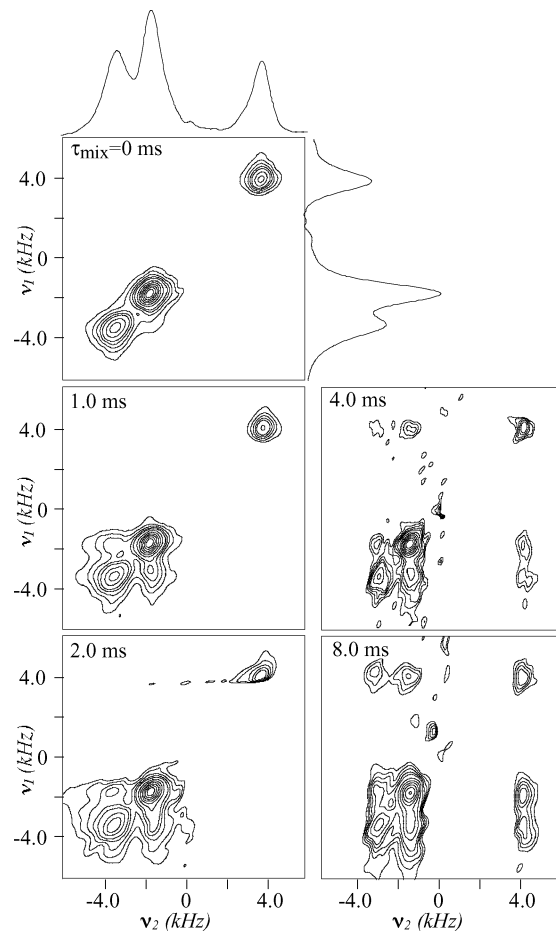


Figure 16. Experimental ^{11}B 2D exchange spectra on $\text{B}_{10}\text{H}_{14}$ at $B_0 = 11.7$ T ($\omega_r/2\pi = -160.732$ MHz) and $\omega_r/2\pi = 15.0$ kHz for various mixing intervals τ_{mix} . TPPM ^1H -decoupling ($\omega_{\text{nuc}}/2\pi = 80$ kHz) was used throughout the various stages of these experiments.

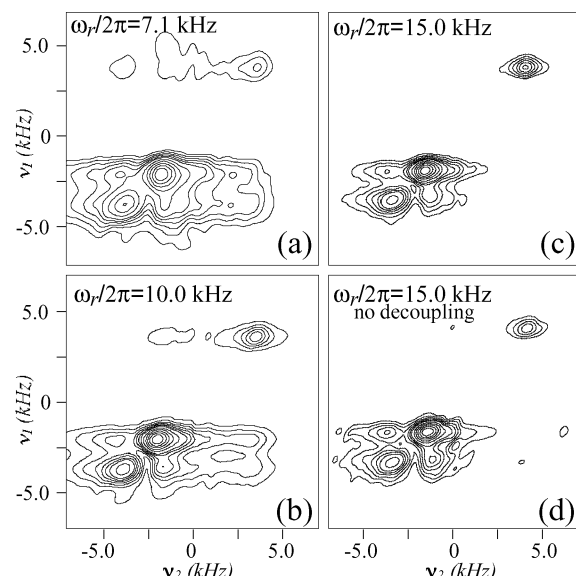


Figure 17. Experimental ^{11}B 2D exchange spectra on $\text{B}_{10}\text{H}_{14}$ at $B_0 = 11.7$ T using a constant mixing interval of $\tau_{\text{mix}} = 2.0$ ms and various spinning frequencies $\omega_r/2\pi$. By contrast to all other 2D contour plots shown in this paper, these spectra are shown after magnitude calculation. TPPM ^1H -decoupling ($\omega_{\text{nuc}}/2\pi \approx 80$ kHz) was used throughout all experiments except during the mixing in (d), where none was applied during the mixing interval.

could lead to the buildup of substantial cross-peak intensities, even at the relatively fast spinning rates used in this work. From

these purely dipolar arguments one might expect that cross-peaks between any pair of peaks in the 2D exchange spectrum would develop at comparable rates. This behavior is not actually supported by the experimental exchange spectra (Figure 16); on the basis of numerical simulations, we rationalize it by the different degrees of overlap exhibited by the three main resonances in the spectrum.

5. Conclusions

The present work explored both theoretically and experimentally a variety of issues concerning the recoupling of half-integer quadrupole nuclei in the solid state, and their monitoring via 2D exchange MAS experiments. The main purpose of the present contribution was to discuss the dissimilar and often competing processes that can assist the spontaneous recoupling of quadrupole systems based on the modulation of anisotropic interactions undergoing MAS, and to illustrate these various contributions by running arrays of experiments on a variety of compounds, external magnetic fields and rotational frequencies. Unfortunately, the chosen spin systems did not allow us to make a step-by-step analysis of the predictions made by a rigorous theory. A main obstacle that prevented us from achieving these comparisons was the multispin nature of the chosen systems. Indeed, whereas isolated pairs of nuclei have long been the trademark of recoupling developments in spin- $1/2$ spectroscopy, such systems are harder to come by when dealing with half-integer quadrupoles. Still, from a qualitative standpoint the compounds used in this study allowed us to identify the differing mechanisms capable of driving spin diffusion for $S \geq 3/2$.

Also worth assessing is the usefulness and limitations of the 2D exchange experiment as a structural tool. On comparing multispin simulations on small systems with the experimental results collected during this study, we observed that the former usually predicted much faster buildup rates for the exchange yet also incomplete ridges that suggest substantial anisotropy. This indicates that exchange experiments will be more useful for retrieving relative tensor orientations, than for the extraction of accurate internuclear distances. A similar limitation has been reported when dealing with multiply labeled systems of spin- $1/2$ nuclei,⁶¹ and it is therefore likely that our observations reflect once again complications arising when dealing with clusters of half-integer quadrupoles. On the other hand, it is likely that when dealing with pairs or triads of coupled nuclei this will not constitute a major problem, provided of course that the origin of the transfer can be determined.

Acknowledgment. We are grateful to Dr. Julia Grinshtein for assistance in recording the data in Figure 15 and to Dr. Christopher V. Grant for providing the chemical shift and quadrupolar parameters of dCMP. This research was supported by a Philip M. Klutznick Fund for Research (Weizmann Institute), by the Minerva Foundation (Munich, FRG), and by the Israeli Science Foundation (grant #296/01). M.E. acknowledges a postdoctoral fellowship from The Swedish Foundation for International Cooperation in Research and Higher Education (STINT).

References and Notes

- (1) Fitzgerald, J. *Solid State NMR of Inorganic Materials*; Fitzgerald, J., Ed.; Washington, DC, 1999.
- (2) Smith, M. E.; vanEck, E. R. H. *Progress NMR Spectrosc.* **1999**, 34, 159.
- (3) *New NMR Techniques for Quadrupolar Nuclei*; Anderson, M. W., Duer, M. J., Eds.; Solid State NMR; 1999; Vol. 15.
- (4) Freude, D. In *Encyclopedia of Analytical Chemistry*; Meyers, R. A., Ed.; J. Wiley & Sons: Chichester, U.K., 2000; p 12188.
- (5) Cohen, M. H.; Reif, F. *Solid State Phys.* **1957**, 5, 321.
- (6) Chmelka, B. F.; Zwanziger, J. W. *NMR Basic Principles Prog.* **1994**, 33, 79.
- (7) Frydman, L. *Annu. Rev. Phys. Chem.* **2001**, 52, 463.
- (8) Wooten, E. W.; Muller, K. T.; Pines, A. *Acc. Chem. Res.* **1992**, 25, 209.
- (9) Frydman, L.; Harwood, J. S. *J. Am. Chem. Soc.* **1995**, 117, 5367.
- (10) Medek, A.; Harwood, J. S.; Frydman, L. *J. Am. Chem. Soc.* **1995**, 117, 12779.
- (11) Gan, Z. H. *J. Am. Chem. Soc.* **2000**, 122, 3242.
- (12) Gan, Z. H. *J. Chem. Phys.* **2001**, 114, 10845.
- (13) Waugh, J. S. *Proc. Natl. Acad. Sci. U.S.A.* **1976**, 73, 1394.
- (14) Stoll, M. E.; Vega, A. J.; Vaughan, R. W. *J. Chem. Phys.* **1976**, 65, 4093.
- (15) Linder, M.; Hohener, A.; Ernst, R. R. *J. Chem. Phys.* **1980**, 73, 4959.
- (16) Griffiths, J. M.; Griffin, R. G. *Anal. Chim. Acta* **1993**, 283, 1081.
- (17) Gullion, T. *Concepts Magn. Reson.* **1998**, 10, 277.
- (18) Dusold, S.; Sebald, A. *Ann. Rep. NMR Spectrosc.* **2000**, 41, 185.
- (19) Baldus, M.; Rovnyak, D.; Griffin, R. G. *J. Chem. Phys.* **1996**, 112, 5902.
- (20) Wi, S.; Logan, J. W.; Sakellariou, D.; Walls, J. D.; Pines, A. *J. Chem. Phys.* **2002**, 117, 7024.
- (21) Nijman, M.; Ernst, M.; Kentgens, A. P. M.; Meier, B. H. *Mol. Phys.* **2000**, 98, 161.
- (22) Joo, C.; Werner-Zwanziger, U.; Zwanziger, J. W. *Solid State NMR* **2000**, 16, 77.
- (23) Ajithkumar, T. J.; Kentgens, A. P. M. *J. Am. Chem. Soc.* **2003**, 125, 2398.
- (24) Ding, S.; McDowell, C. A. *Mol. Phys.* **1995**, 85, 283.
- (25) Duer, M. J. *Chem. Phys. Lett.* **1997**, 277, 167.
- (26) Gan, Z.; Robyr, P. *Mol. Phys.* **1998**, 95, 1143.
- (27) Duer, M. J.; Painter, A. J. *Chem. Phys. Lett.* **1999**, 313, 763.
- (28) Rovnyak, D.; Baldus, M.; Wu, G.; Hud, N. V.; Feigson, J.; Griffin, R. G. *J. Am. Chem. Soc.* **2000**, 122, 11423.
- (29) Facey, G.; Gusev, D.; Morris, R. H.; Macholl, S.; Buntkowsky, G. *Phys. Chem. Chem. Phys.* **2000**, 2, 935.
- (30) Edén, M.; Frydman, L. *J. Chem. Phys.* **2001**, 114, 4116.
- (31) Dowell, N. G.; Ashbrook, S. E.; McManus, J.; Wimperis, S. *J. Am. Chem. Soc.* **2001**, 123, 8135.
- (32) Dowell, N. G.; Ashbrook, S. E.; Wimperis, S. *J. Phys. Chem. A* **2002**, 106, 9470.
- (33) Edén, M.; Grinshtein, J.; Frydman, L. *J. Am. Chem. Soc.* **2002**, 124, 9708.
- (34) Lefebvre, F.; Amoureaux, J. P.; Fernandez, C.; Derouane, E. G. *J. Chem. Phys.* **1987**, 86, 6070.
- (35) Edén, M. *Concepts Magn. Reson.* **2003**, 17A, 117.
- (36) Maricq, M. M.; Waugh, J. S. *J. Chem. Phys.* **1979**, 70, 3300.
- (37) Levitt, M. H.; Raleigh, D. P.; Creuzet, F.; Griffin, R. G. *J. Chem. Phys.* **1990**, 92, 6347.
- (38) Kubo, A.; McDowell, C. A. *J. Chem. Phys.* **1990**, 92, 7156.
- (39) Haebler, U. In *Advances in Magnetic Resonance*; Waugh, J. S., Ed.; Academic Press: New York, 1976.
- (40) Herzfeld, J.; Berger, A. E. *J. Chem. Phys.* **1980**, 73, 6021.
- (41) Eichele K.; Wu, G.; Wasylissen, R. E. *J. Magn. Reson. A* **1993**, 101, 157.
- (42) Brunner, E.; Freude, D.; Gerstein, B. C.; Pfeifer, H. *J. Magn. Reson.* **1990**, 90, 90.
- (43) Wi, S.; Frydman, L. *J. Chem. Phys.* **2000**, 112, 3248.
- (44) Raleigh, D. P.; Levitt, M. H.; Griffin, R. G. *Chem. Phys. Lett.* **1988**, 146, 71.
- (45) Schmidt-Rohr, K.; Spiess, H. W. *Multidimensional Solid-State NMR and Polymers*; Academic Press: London, 1994.
- (46) Edén, M.; Lee, Y. K.; Levitt, M. H. *J. Magn. Reson. A* **1996**, 120, 56.
- (47) Jeener, J.; Meier, B. H.; Bachmann, P.; Ernst, R. R. *J. Chem. Phys.* **1979**, 71, 4546.
- (48) Henrichs, P. M.; Linder, M. *J. Magn. Reson.* **1984**, 58, 458.
- (49) Tycko, R.; Dabbagh, G. *J. Am. Chem. Soc.* **1991**, 113, 3592.
- (50) Bennett, A. E.; Rienstra, C. M.; Auger, M.; Lakshmi, K. V.; Griffin, R. G. *J. Chem. Phys.* **1995**, 103, 6951.
- (51) Catti, A.; Ferraris, G.; Franchini-Angela, M. *Acta Crystallogr.* **1977**, B33, 3449.
- (52) Pandit, J.; Seshadri, T. P.; Viswamitra, M. A. *Acta Crystallogr.* **1983**, C39, 342.
- (53) Grinshtein, J.; Grant, C. V.; Frydman, L. *J. Am. Chem. Soc.* **2002**, 124, 13344.

(54) Wong, A.; Wu, G. *J. Phys. Chem. A* **2003**, *107*, 579.
(55) Larsen, L. O.; Kierkegaard, P. *Acta Chem. Scand.* **1969**, *23*, 2253.
(56) Power, W. P. *Magn. Reson. Chem.* **1994**, *33*, 220.
(57) Gurr, G. E.; Montgomery, P. W.; Knutson, C. D.; Gorres., B. T. *Acta Crystallogr.* **1970**, *B26*, 906.
(58) Kasper, J. S.; Lucht, C. M.; Harker, D. *Acta Crystallogr.* **1950**, *3*, 436.
(59) Clouse, A. O.; Moody, D. C.; Rietz, R. R.; Rospberry, T.; Schaeffer, R. *J. Am. Chem. Soc.* **1973**, *95*, 2496.
(60) Grinshtein, J.; Frydman, L. *J. Am. Chem. Soc.* **2003**, *125*, 7451.
(61) Hodgkinson, P.; Emsley, L. *J. Magn. Reson.* **1999**, *139*, 46.
(62) Conroy, H. C. *J. Chem. Phys.* **1967**, *47*, 5307.
(63) Cheng, V. B.; Suzukawa, H. H.; Wolfsberg, M. *J. Chem. Phys.* **1973**, *59*, 3992.